Supporting Information

Ambipolar Transport in Two-Dimensional Sn-Based Perovskite Field-Effect Transistors Using an Aliphatic Polymer-Assisted Method

Fan Zhang, Quan Zhang, Xin Liu, Liang Qin, Yufeng Hu, Zhidong Lou*, Yanbing Hou and Feng Teng*

Key Laboratory of Luminescence and Optical Information, Ministry of Education, Beijing Jiaotong University, Beijing 100044, China

*Corresponding authors at: Key Laboratory of Luminescence and Optical Information, Ministry of Education, Beijing Jiaotong University, Beijing 100044, China.

Tel.: +86 10 5168 4860

Electronic mails: zhdlou@bjtu.edu.cn and fteng@bjtu.edu.cn

Crystal Structure and Morphology
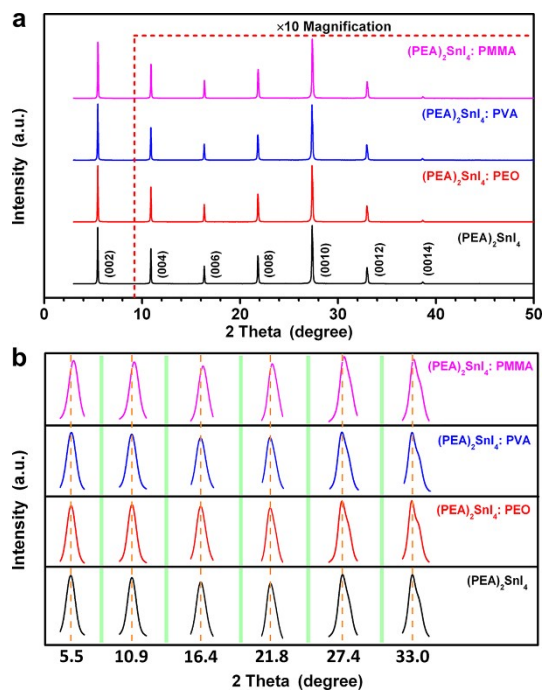
Figure S1. (a) Normalized XRD patterns and (b) magnified XRD peaks of the $(PEA)_2SnI_4$ and aliphatic polymer-assisted $(PEA)_2SnI_4$ thin films.
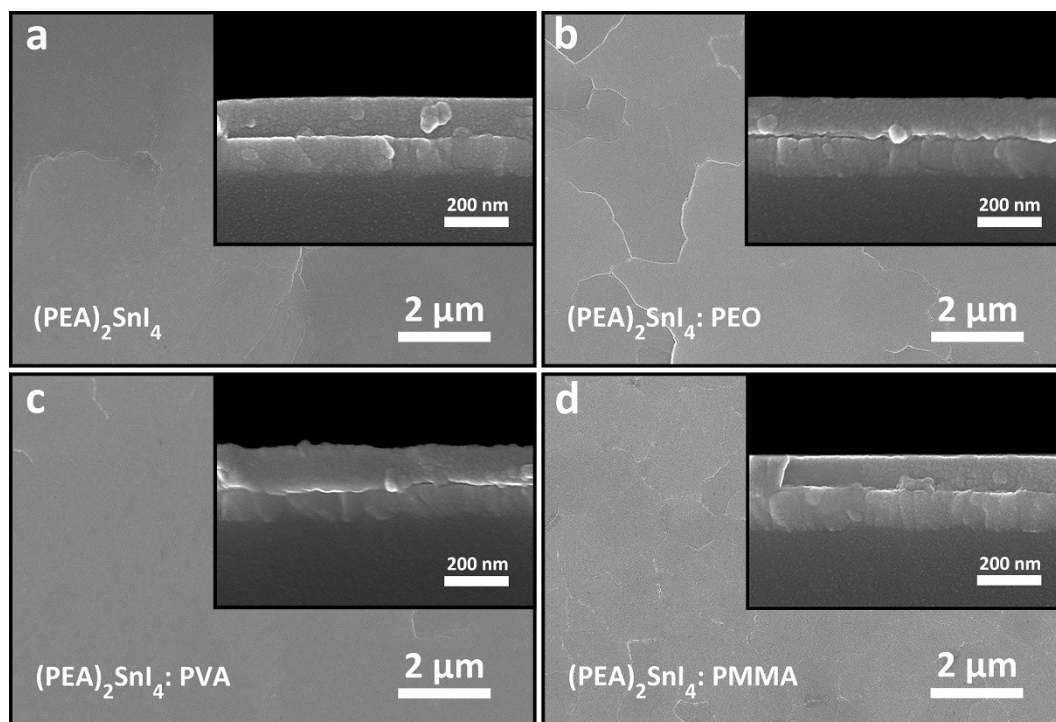
Figure S2. Top-view SEM images of the (a) $(PEA)_2SnI_4$ and (b-d) aliphatic polymer-assisted $(PEA)_2SnI_4$ thin films. The insets show the cross-sectional SEM images of these perovskite films.

Intermolecular Interactions
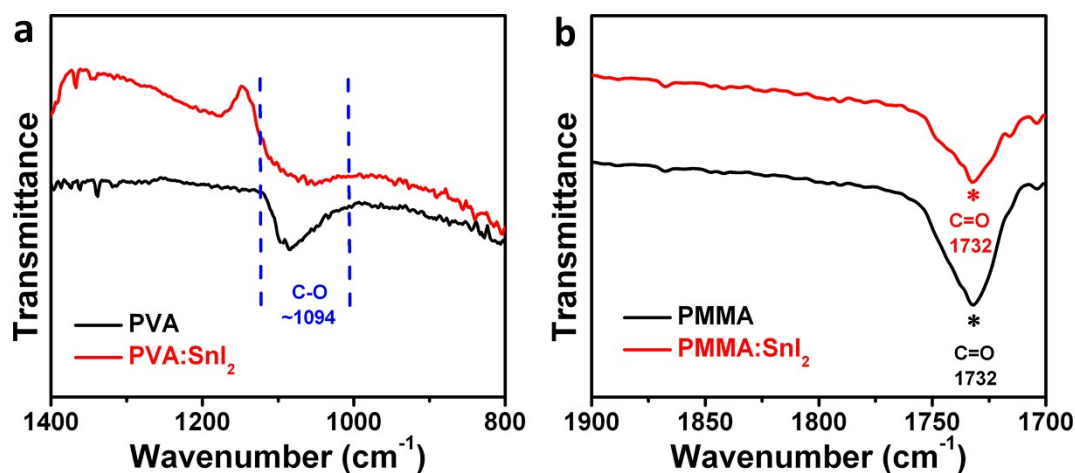
Figure S3. FTIR spectra of (a) the pristine PVA and PVA: SnI_2 composite films and (b) the pristine PMMA and PMMA: SnI_2 composite films.
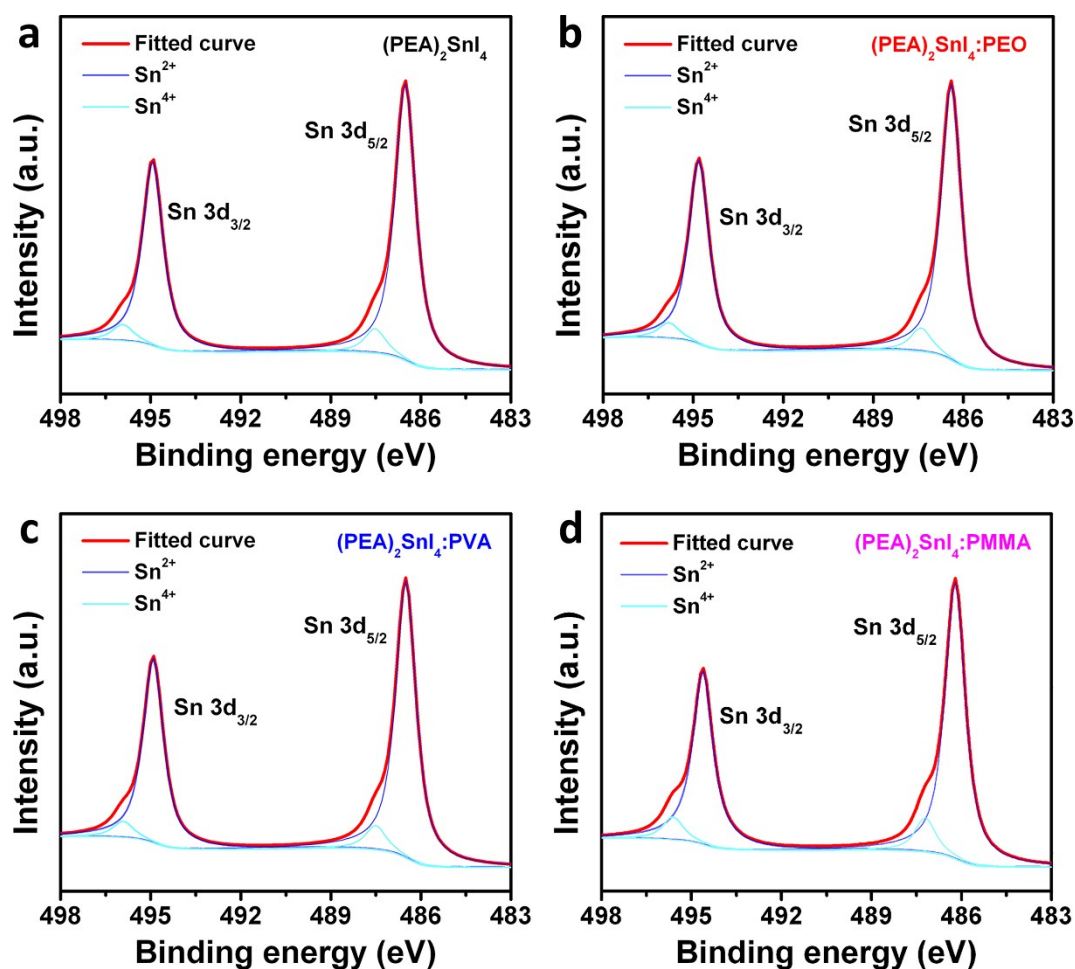
Figure S4. XPS spectra of the Sn element in (a) the $(PEA)_2SnI_4$ and (b-d) aliphatic polymer-assisted $(PEA)_2SnI_4$ thin films.

Electronic Bandgap Structure
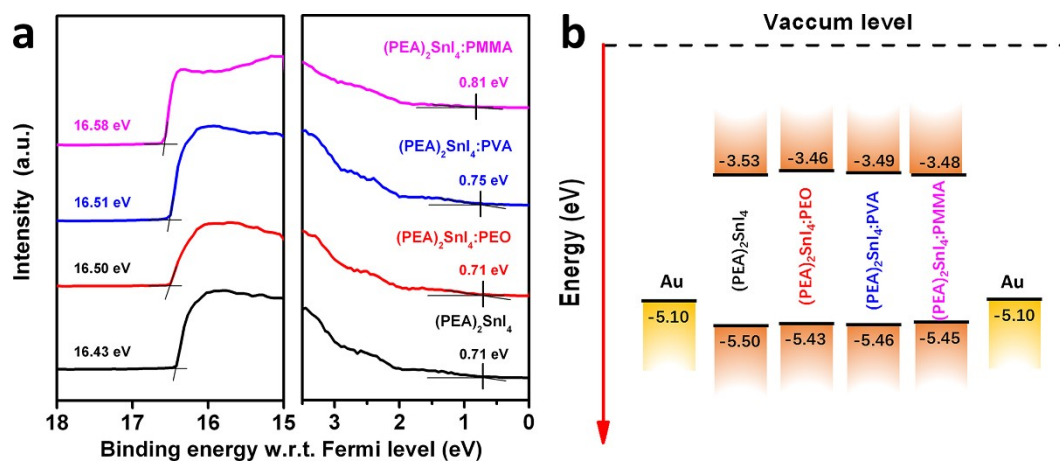
Figure S5. (a) UPS spectra, and (b) energy level structures of the (PEA)$_2$SnI$_4$ and aliphatic polymer-assisted (PEA)$_2$SnI$_4$ thin films.

Carrier Lifetime

The time-resolved PL intensity (I_{PL}) can be fitted by the following three-variable parameter exponential function:

$$I_{PL} = A_1\exp\left(-t/\tau_1\right) + A_2\exp\left(-t/\tau_2\right) + A_3\exp\left(-t/\tau_3\right),$$

where τ_i refers to the time constant of each exponential component, and A_i is the fractional amplitude for each exponential. In this model, there are three processes dominating the charge-carrier recombination in perovskites: trap-related non-radiative recombination, auger recombination, and radiative recombination, corresponding to τ_1, τ_2, and τ_3, respectively. The average carrier lifetime can be given by the following equation:

$$\tau_{ave} = \frac{A_1\tau_1^2 + A_2\tau_2^2 + A_3\tau_3^2}{A_1\tau_1 + A_2\tau_2 + A_3\tau_3}.$$

The amplitude-weighted average lifetimes offer greater accuracy because of taking the contraharmonic mean of each component.

Table S1. Carrier lifetimes of the $(PEA)_2SnI_4$ and aliphatic polymer-assisted $(PEA)_2SnI_4$ thin films fitted with a three-exponential decay model. The average and standard deviation values in the parentheses are evaluated based on the results of three-time measurements.

	τ_1 (ns)	τ_2 (ns)	τ_3 (ns)	τ_{ave} (ns)
$(PEA)_2SnI_4$	4.50 (4.79±0.93)	17.20 (16.10±1.15)	1.20 (1.37±0.18)	2.35 (2.24±0.13)
$(PEA)_2SnI_4$: PEO	8.05 (7.31±0.82)	27.20 (14.10±9.28)	2.10 (2.00±0.33)	4.35 (4.30±0.05)
$(PEA)_2SnI_4$: PVA	4.37 (3.73±0.67)	16.6 (14.60±6.52)	1.14 (1.19±0.08)	2.23 (2.01±0.17)
$(PEA)_2SnI_4$: PMMA	4.71 (5.15±0.65)	15.4 (14.80±6.12)	1.24 (1.40±0.10)	2.78 (2.61±0.46)

Field-Effect Transistors
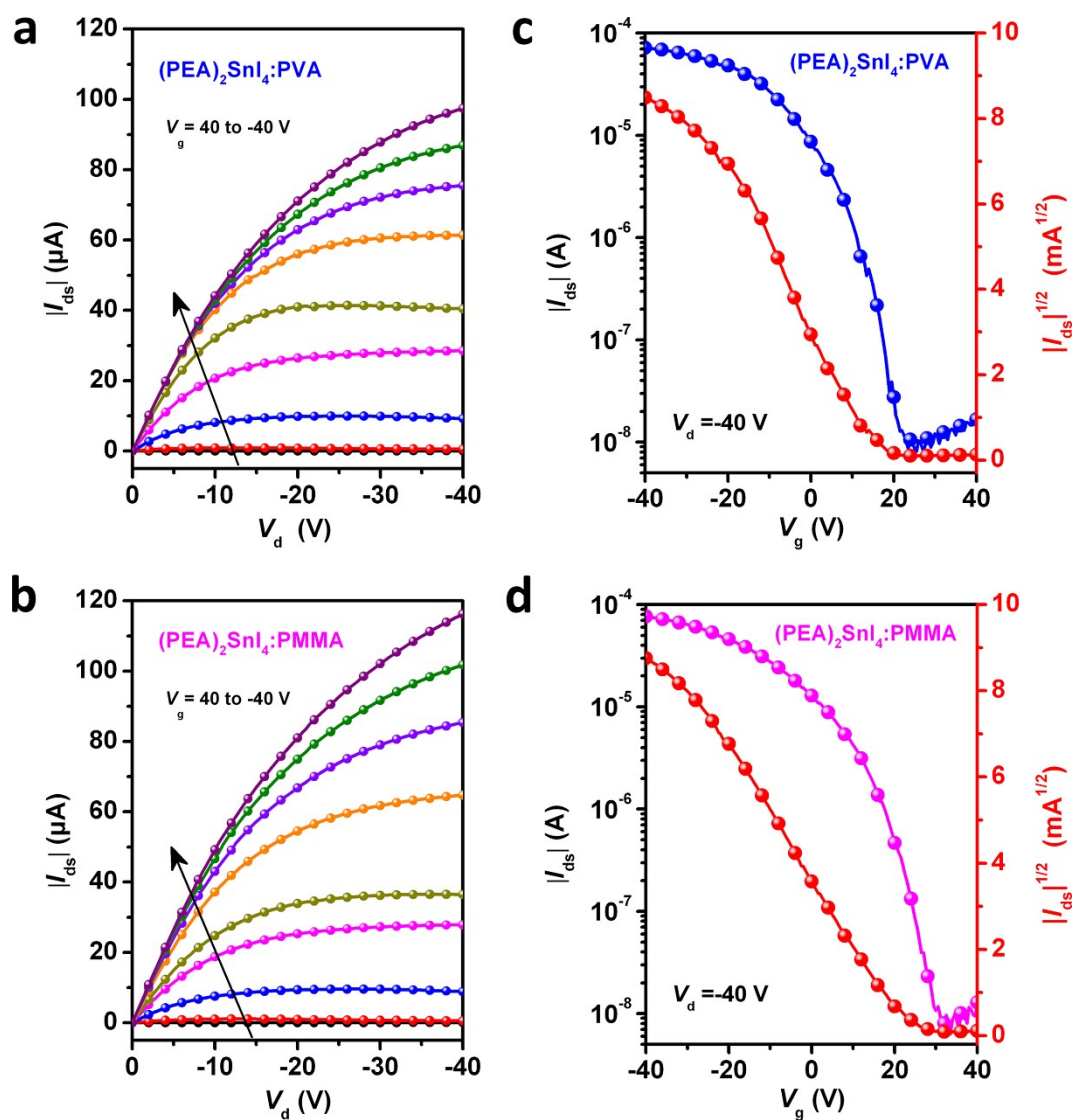
Figure S6. Output and transfer characteristics of the (a, b) $(PEA)_2SnI_4$: PVA and (c, d) $(PEA)_2SnI_4$: PMMA field-effect transistors.
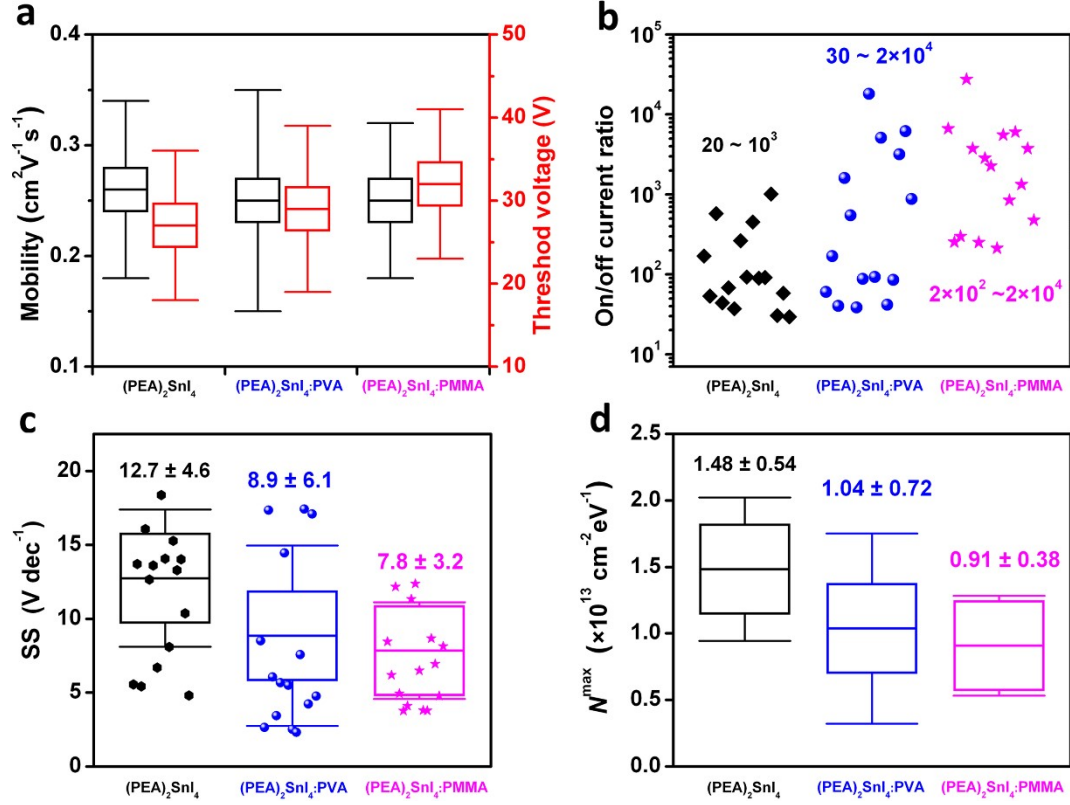
Figure S7. (a) Mobility and threshold voltage (average values with standard deviations), (b) on/off current ratio (scatter diagram), (c) subthreshold swing (average values with standard deviations and scatter diagram), and (d) maximum interface trap density (average values with standard deviations) of fifteen $(PEA)_2SnI_4$ transistors, fifteen $(PEA)_2SnI_4$: PVA transistors, and fifteen $(PEA)_2SnI_4$: PMMA transistors.

Table S2. Device parameters and maximum interface trap state densities of the $(PEA)_2SnI_4$, $(PEA)_2SnI_4$: PVA, and $(PEA)_2SnI_4$: PMMA transistors. The values in the parentheses are the average ones with standard deviations derived from fifteen devices for each type of transistors.

Perovskite	Mobility $(cm^2V^{-1}s^{-1})$	Threshold voltage (V)	On-off current ratio	Subthreshold slope $(Vdec^{-1})$	Maximum interface trap density $(\times 10^{13}\ cm^{-2}eV^{-1})$
$(PEA)_2SnI_4$	0.45 (0.26 ± 0.08)	12 (27 ± 9)	~10^3	16.0 (12.7 ± 4.6)	1.87 (1.48 ± 0.54)
$(PEA)_2SnI_4$: PVA	0.44 (0.25 ± 0.10)	13 (29 ± 10)	~10^4	6.1 (8.9 ± 6.1)	0.71 (1.04 ± 0.72)
$(PEA)_2SnI_4$: PMMA	0.25 (0.25 ± 0.07)	22 (32 ± 9)	~10^4	5.6 (7.8 ± 3.2)	0.65 (0.91 ± 0.38)

Water Contact Angles
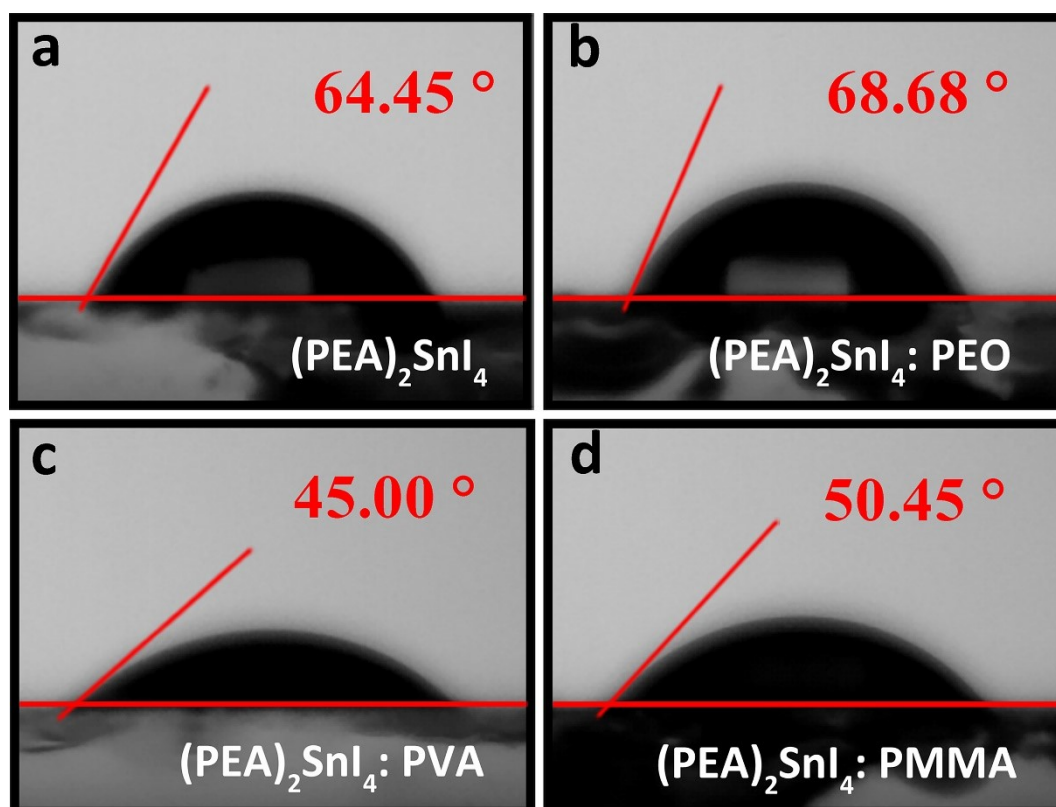
Figure S8. Water contact angles of the (a) $(PEA)_2SnI_4$ and (c-d) aliphatic polymer-assisted $(PEA)_2SnI_4$ thin films.

Table S3. Water contact angles of the $(PEA)_2SnI_4$ and aliphatic polymer-assisted $(PEA)_2SnI_4$ thin films.

	$(PEA)_2SnI_4$	$(PEA)_2SnI_4$: PEO	$(PEA)_2SnI_4$: PVA	$(PEA)_2SnI_4$: PMMA
Water contact angle (º)	64.45	68.68	45.00	50.45
	62.88±1.73	66.85±1.80	36.51±4.61	47.83±2.68
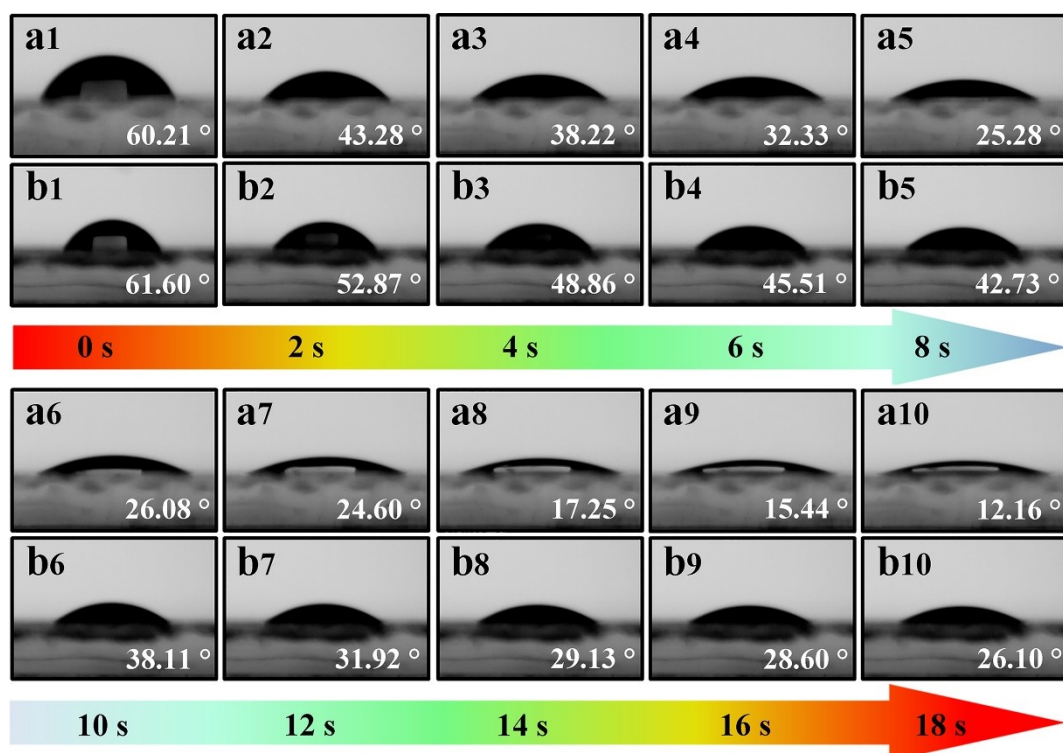
Figure S9. Water contact angles of the $(PEA)_2SnI_4$ (a1-a10) and $(PEA)_2SnI_4$: PEO (b1-b10) thin films over time.

The water contact angle measurements were performed on the pristine $(PEA)_2SnI_4$ and polymer-assisted $(PEA)_2SnI_4$ thin films in order to evaluate their resistance to water, which can accelerate the oxidation of Sn^{2+}. As depicted in Figure S9, the larger contact angle of the $(PEA)_2SnI_4$: PEO film (68.68 °) compared with that of the $(PEA)_2SnI_4$ film (64.45 °) reveals that the PEO chains distributed at the grain boundaries and the surface can effectively enhance the resistance to water due to the strong hydrogen bonds and coordination interactions between PEO and $(PEA)_2SnI_4$, effectively suppressing the infiltration of water and oxygen along the grain boundaries. Nevertheless, the contact angles of the $(PEA)_2SnI_4$: PVA and $(PEA)_2SnI_4$: PMMA films decline to 45.00 ° and 50.45 °, respectively, which is ascribed to the hydrophilic hydroxyl groups (-OH) of PVA in $(PEA)_2SnI_4$: PVA and the impact of the ester carbonyl groups of PMMA on the crystallization of $(PEA)_2SnI_4$: PMMA. Additionally,

the average water contact angles with standard deviations estimated by measuring each perovskite film with five times are summarized in Table S3, which presents the same change trend. To further assess the effect of PEO, the changes of the water contact angles of the $(PEA)_2SnI_4$ and $(PEA)_2SnI_4$: PEO films over time were recorded and exhibited in Figure S10. The water contact angle of the $(PEA)_2SnI_4$: PEO film decreases from 61.60 ° to 26.10 ° within 18 s, while that of the $(PEA)_2SnI_4$ film rapidly drops from 60.21 ° to 12.19 °, indicating that PEO can effectively enhance the water resistance of the perovskite film in spite of its hydrophilicity.

AC Impedance Spectra

An AC impedance spectroscopy technique is utilized to explore the physical processes in the vertical direction in the perovskite field-effect transistors. By connecting the ITO gate electrode and one of the Au electrodes of the transistors to the impedance analyzer, the Nyquist plots (Figure 5(a)) of the MIS capacitors in the pure $(PEA)_2SnI_4$, $(PEA)_2SnI_4$: PEO, $(PEA)_2SnI_4$: PVA, and $(PEA)_2SnI_4$: PMMA device were recorded in the dark with an applied AC signal of 500 mV and no DC bias. The electrical parameters of the corresponding circuit elements are obtained by fitting the impedance spectra and listed in Table S1. The electrical parameters (Table S4) in the equivalent circuits in Figure 5(c) are extracted by fitting the corresponding circuits to the impedance spectra in Figure 5(a). Here, R_S represents the resistive loss in the circuits; the constant phase element (CPE) is a capacitive element originating from non-ideal materials or interfaces, which comprises CPE-T and CPE-P.[1] CPE-T is a quasi-capacitor, and CPE-P represents an ideality factor with its value changing from 0 to 1. In Figure 5(c) the only one RC loop (R and CPE in parallel) for the MIS capacitor in the $(PEA)_2SnI_4$: PEO transistor matches the only one semi-circular arc in its Nyquist plot (Figure 5(a)). The parallel R_1 and CPE1 (R_1C_1) as well as R_2 and CPE2 (R_2C_2) correspond to the two semicircles in the Nyquist plots of the $(PEA)_2SnI_4$, $(PEA)_2SnI_4$: PVA, and $(PEA)_2SnI_4$: PMMA devices. The RC loops at different frequencies in the equivalent circuits represent different physical processes occurring on different time scales. The equivalent capacitance C of each CPE can be estimated with the following formula[2]

$$C = \frac{(RCPE\text{-}T)^{\frac{1}{CPE\text{-}P}}}{R}.$$

To further understand the different physical processes in the perovskite transistors,

the relaxation time τ of each RC circuit can be derived according to the following

formula[2]

$$\frac{1}{\tau} = \frac{1}{RC}.$$

Table S4. Electrical parameters of the elements in the equivalent circuits extracted by fitting the impedance spectra of the MIS capacitors in the $(PEA)_2SnI_4$ and aliphatic polymer-assisted $(PEA)_2SnI_4$ transistors at 0 V. CPE-T is a quasi-capacitor, and CPE-P represents an ideality factor with a value between 0 and 1.

Device	Rs (Ω)	R_1 ($\times 10^5$ Ω)	CPE1-T ($\times 10^{-10}$ F)	CPE1-P	R_2 (MΩ)	CPE2-T ($\times 10^{-10}$ F)	CPE2-P
$(PEA)_2SnI_4$	59	1.80	4.10	0.92	9.90	1.95	0.92
$(PEA)_2SnI_4$: PEO	64	141	6.17	0.90	--	--	--
$(PEA)_2SnI_4$: PVA	67	5.10	2.89	0.96	4.30	3.80	0.85
$(PEA)_2SnI_4$: PMMA	67	5.50	4.60	0.94	12.0	3.50	0.84

Table S5. Equivalent capacitance and relaxation time for the RC circuits in the $(PEA)_2SnI_4$, $(PEA)_2SnI_4$: PVA, and $(PEA)_2SnI_4$: PMMA transistors at 0 V.

	C_1 (nF)	C_2 (nF)	τ_1 (μs)
$(PEA)_2SnI_4$	0.18	1.58	32.3
$(PEA)_2SnI_4$: PVA	0.20	1.84	102.1
$(PEA)_2SnI_4$: PMMA	0.27	1.91	149.1

The gate leakage current
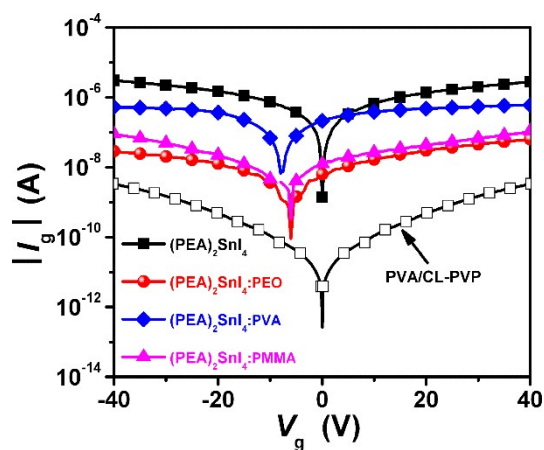
Figure S10. The gate leakage currents of the $(PEA)_2SnI_4$, $(PEA)_2SnI_4$: PEO, $(PEA)_2SnI_4$: PVA, and $(PEA)_2SnI_4$: PMMA field-effect transistors and the leakage current of the Au/PVA/CL-PVP/ITO device.

Reference

1. J. Lin, M. Weis, D. Taguchi, T. Manaka and M. Iwamoto, *Thin Solid Films*, 2009, **518**, 448-451.

2. B. J. Leever, C. A. Bailey, T. J. Marks, M. C. Hersam and M. F. Durstock, *Adv. Energy Mater.*, 2012, **2**, 120-128.